Biomaterial Immobilization in Nanoporous Carbon Molecular Sieves: Influence of Solution pH, Pore Volume, and Pore Diameter

Ajayan Vinu,*,† Masahiko Miyahara,‡ and Katsuhiko Ariga‡

International Center for Young Scientists and Supermolecules Group, Advanced Materials Laboratory, National Institute for Materials Science, 1-1 Namiki, Tsukuba, Ibaraki 305-0044, Japan

Received: January 26, 2005; In Final Form: February 5, 2005

The adsorption of lysozyme (Lz) onto nanoporous carbon molecular sieves with various pore diameters has been studied at different solution pH values. All the adsorption isotherms have successfully been correlated by the Langmuir equation. The amount of adsorbed Lz depends on the solution pH as well as on the specific pore volume and pore diameter of the adsorbents. The maximum adsorption was observed near the isoelectric point of the Lz (pI $\approx$ 11), suggesting that suppression of electric repulsion between the enzymes plays an important role in the adsorption process. Moreover, the amount adsorbed depends on the pore size and pore volume of the nanoporous carbon adsorbents, indicating that the Lz molecules are adsorbed inside the mesopores. CMK-3-150 shows a larger amount of Lz adsorption as compared to CMK-3. The increased Lz adsorption capacity of CMK-3-150 may be due to the larger pore volume and pore diameter as compared to that of CMK-3. The unaltered structural order of the nanoporous adsorbents after the adsorption has been confirmed by the physicochemical characterization techniques such as XRD and N_2 adsorption. In addition, FT-IR spectroscopic studies confirm that the Lz used in this study is stable even after the adsorption on the nanoporous carbon. These results indicate that nanoporous carbon has superior water stability and thus is a more appropriate adsorbent for biomaterials than nanoporous silica.

Introduction

The immobilization of biomolecules such as proteins and peptides onto solid supports has attracted much attention due to its scientific importance and application in many areas, such as biology, medicine, biotechnology, and food processing.[1−4] Especially, use of nanoorganized materials as the supports leads to development of nanosize reactors[5,6] and sensors.[7,8] Among the nanoorganized materials, mesoporous materials have obtained considerable attention in the adsorption of large molecules such as enzymes and vitamins due to their well-ordered pore structure with high specific surface area and pore volume.[9−24] Very recently, Vinu et al. have reported the adsorption of cytochrome *c* and lysozyme (Lz) over various mesoporous silica molecular sieves.[25,26] However, for these materials, strong electrostatic interactions are observed between the surface silanol groups and the surface charge on the amino acid residues on the surface of the protein molecule which may damage the native state of a protein molecule and lead to the loss of its coherent structure. In addition, the structural stability of the mesoporous silica adsorbent after adsorption is relatively poor due to the hydrolysis of their siloxane bridges. The efficiency of biochemical devices, which are made from the protein immobilized solid supports, ranging from drug delivery devices to contact lenses, tissue culture scaffolds, and biosensors, relies heavily on the stability of solid adsorbents and solid protein interactions. Thus, we realized that use of a thermally, mechanically, and water stable mesoporous material is indispensable for future development of nanobiomedical devices.

As the next generation of mesoporous materials, nanoporous carbon has been paid much attention due to its application in many areas, such as gas separation, adsorption of small gas molecules, catalysis, energy storage, and capacitors.[27−32] Ryoo et al. prepared ordered nanoporous carbons (CMK-*x*) from mesoporous silica templates such as MCM-48, SBA-1, and SBA-15 using sucrose as the carbon source.[28,30−32] Independently and somewhat later, Hyeon et al. have used similar approaches and prepared mesoporous carbon materials, designated as SNU-*x*.[29,33] Recently, Vinu et al. have also reported the preparation of nanoporous carbon with variable pore diameters using SBA-15 materials synthesized at different temperatures.[34] These materials possess well-ordered pore structure, very high specific pore volume, specific surface area, and tunable pore diameter. They have also no charge on their surface and are highly tolerant in aqueous environment compared with silica materials. Very recently, Han et al.[35] have reported the adsorption of humic acids over nanoporous carbon materials which were prepared from silica sol particles as the template. These materials showed higher and faster adsorption of humic acids than the commercial activated carbons such as F400 and Norit SA. Despite such potential capability of the nanoporous carbon materials, there has been only a limited number of works on the adsorption of large biomolecules such as vitamins and proteins over nanoporous carbon molecular sieves.

In the present contribution, we report here for the first time the adsorption of Lz,[25] which has a prolate spheroid shape with two characteristic cross sections: a side of dimensions of roughly 3.0 × 4.5 nm^2 and an end of dimensions 3.0 × 3.0 nm^2, over nanoporous carbon molecular sieves with different specific surface area, specific pore volume, and pore diameter. It has been found that the amount of adsorption mainly depends

* To whom correspondence should be addressed. Phone: +81-29-851-3354 (ext. 8679); +81-29-860-4706. E-mail: vinu.ajayan@nims.go.jp.
† International Center for Young Scientists.
‡ Supermolecules Group.

10.1021/jp050454o CCC: $30.25
Published on Web 03/11/2005

on the solution pH as well as the specific pore volume and pore diameter of the nanoporous carbon adsorbent. Among the carbon materials studied, CMK-3-150 shows a higher amount of Lz adsorption as compared to the other nanoporous carbons such as CMK-1, CMK-3, and CMK-3-130. The XRD, N_2 adsorption, and FT-IR spectroscopic results of the Lz immobilized nanoporous carbon materials confirm that the carbon adsorbents and the protein molecule are highly stable even after the protein adsorption.

Experimental Section

Materials. Tetraethyl orthosilicate, sucrose, and triblock copolymer poly(ethylene glycol)-*block*-poly(propylene glycol)-*block*-poly(ethylene glycol) (Pluronic P123, molecular weight = 5800, $EO_{20}PO_{70}EO_{20}$) were obtained from Aldrich. Potassium phosphate, sodium carbonate, potassium chloride, and sodium hydroxide for buffer preparation were purchased from Wako Pure Chem. Chicken egg white Lz (E.C. 3.2.1.17) was obtained from Sigma and used without further purification.

Preparation of Nanoporous Carbons with Various Pore Diameters. Nanoporous carbons with different pore diameters (CMK-3-*X*) were prepared by using SBA-15-*X* (*X* denotes the synthesis temperature of the mesoporous silica) materials as templates and sucrose as the carbon source. The synthesized materials were designated as CMK-3, CMK-3-130, and CMK-3-150. The template materials were synthesized by using a triblock copolymer template (Pluronic P123) and the detailed procedure has been described elsewhere.[14] In a typical synthesis of nanoporous carbon, 1 g of template (mesoporous silica material) was added to a solution obtained by dissolving 1.25 g of sucrose and 0.14 g of H_2SO_4 in 5 g of water, and keeping the mixture in an oven for 6 h at 100 °C. Subsequently, the oven temperature was raised to 160 °C for another 6 h. To obtain fully polymerized and carbonized sucrose inside the pores of the silica template, 0.8 g of sucrose, 0.09 g of H_2SO_4, and 5 g of water were again added to the pretreated sample and the mixture was again subjected to the thermal treatment described above. The template−polymer composites were then pyrolyzed in a nitrogen flow at 877 °C and kept under these conditions for 6 h to carbonize the polymer. The nanoporous carbon was recovered after dissolution of the silica framework in 5 wt % hydrofluoric acid, by filtration, washed several times with ethanol, and dried at 120 °C. CMK-1 was synthesized by using MCM-48 as the template and sucrose as the carbon source by a similar procedure as used for the synthesis of CMK-3.[31,32]

Characterization. The powder X-ray diffraction (XRD) patterns of nanoporous carbon materials were collected on a Rigaku diffractometer with use of Cu Kα (λ = 0.154 nm) radiation. The diffractograms were recorded in the 2θ range of 0.8° to 10° with a 2θ step size of 0.01° and a step time of 10 s. Nitrogen adsorption and desorption isotherms were measured at −196 °C on a Quantachrome Autosorb 1 sorption analyzer. All samples before protein adsorption were outgassed at 250 °C for 3 h prior to the nitrogen adsorption measurements, while the protein adsorbed samples were outgassed at 40 °C for 24 h. The specific surface area was calculated with use of the Brunauer−Emmett−Teller (BET) method. The pore size distributions were obtained from the adsorption and desorption branch of the nitrogen isotherms by both the Barrett−Joyner−Halenda and the Nonlocal Density Functional Theory (NLDFT) methods. HRTEM images were obtained with TEM JEOL JEM-2000EX2. The preparation of samples for HRTEM analysis involved sonication in ethanol for 2 to 5 min and deposition on a copper grid. The accelerating voltage of the electron beam was 200 kV. FT-IR spectra of CMK-3 before and after the protein adsorption were recorded on a Nicolet Nexus 670 instrument by averaging 200 scans with a resolution of 2 cm^{-1} measuring in transmission mode by using the KBr self-supported pellet technique. The spectrometer chamber was continuously purged with dry air to remove water vapor.

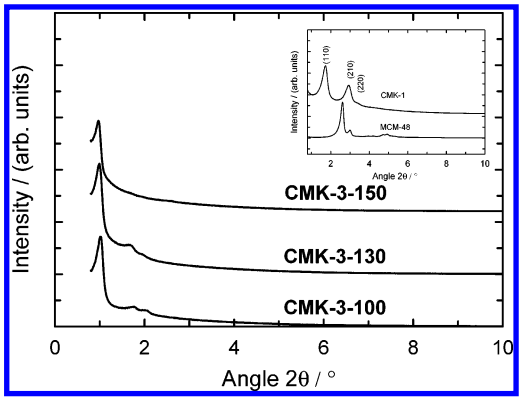

Figure 1. The powder XRD diffraction patterns of different nanoporous carbon adsorbents.

Lysozyme (Lz) Adsorption. A series of standard Lz solutions with concentrations ranging from 17 μ to 280 μmol/L was prepared by dissolving different amounts of Lz in 25 mM buffer solutions (pH 6.5 potassium phosphate buffer, pH 9.6 and 11 sodium bicarbonate buffer, and pH 12 potassium chloride buffer). In each adsorption experiment, 20 mg of the different nanoporous adsorbents was suspended in 4 g of the respective Lz solution. The resulting mixture was continuously shaken in a shaking bath with a speed of 160 shakes/min at 20 °C until equilibrium was reached (typically 96 h for the different nanoporous carbons used in this study). The amount of Lz adsorbed was calculated by subtracting the amount found in the supernatant liquid after adsorption from the amount of Lz present before addition of the adsorbent by UV absorption at 281.5 nm. Calibration experiments were done separately before each set of measurements with Lz solutions of different concentrations buffered at the same pH as the isotherm. Centrifugation prior to the analysis was used to avoid potential interference from suspended scattering particles in the UV−vis analysis.

Results and Discussion

Adsorbent Characterization. The powder X-ray diffraction patterns of CMK-3-100, CMK-3-130, and CMK-3-150 confirm that these materials are hexagonally ordered mesostructures, as evident from the presence of at least three XRD peaks indexed to (100), (110), and (200) reflections (Figure 1). Consequently, the synthesized materials are replicas of the parent material SBA-15.[14] It is interesting to note that the *d* spacing of the nanoporous carbon synthesized with different pore diameters of SBA-15 materials as templates increases in the following order: CMK-3-150 > CMK-3-130 > CMK-3. CMK-1 also exhibits three reflections in the region 2θ = 2° to 3.5° which are indexed to (110), (211), and (220) reflections of the cubic space group $I_1$32 (Figure 1). The XRD pattern of the material before the silica removal is similar to that of MCM-48, which indicates an analogous structure. However, after the removal of the silica template, CMK-1 has an additional relatively narrow (110) diffraction line in its diffraction pattern confirming that the structure of MCM-48 is transformed into another structure (Figure 1).[36]

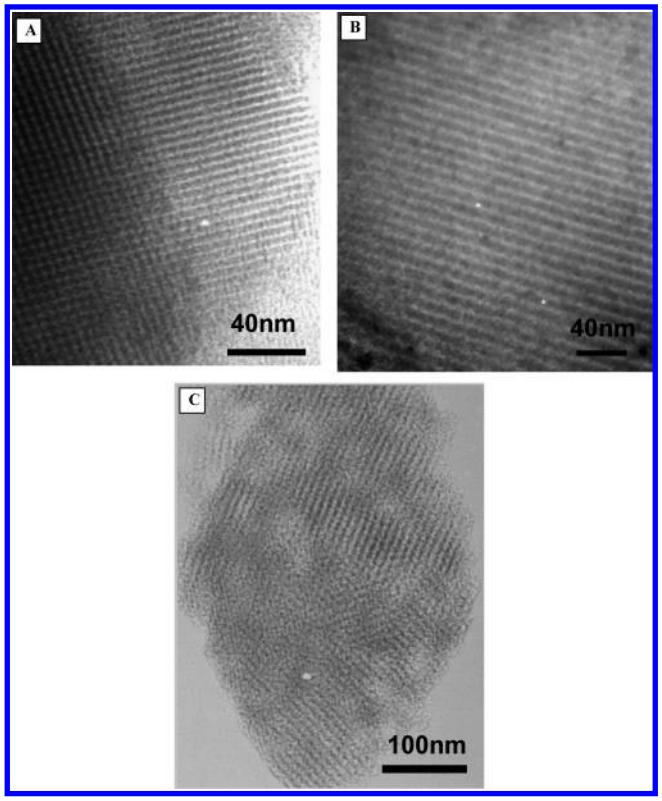

Figure 2. HRTEM images of (A) CMK-1, (B) CMK-3-100, and (C) CMK-3-130.

TABLE 1: Structural Characteristics of the Nanoporous Carbons Used in This Study

adsorbents	*d* spacing (nm)	A_{BET} (m^2/g)	V_p (cm^3/g)	$d_{p,BJH}$ (nm)[a]	$d_{p,NLDFT}$ (nm)[b]
CMK-1	5.14^{d210}	1675	1.05	2.3	
CMK-3-100	8.72	1260	1.10	3.0	3.3
CMK-3-130	9.05	1250	1.30	4.3	4.3
CMK-3-150	9.32	1350	1.60	6.5	5.4

[a] Calculated from the adsorption branch of the isotherm. [b] Pore size obtained from the N_2 isotherm on the basis of nonlocal density functional.

To confirm the mesoporous nature of the different mesoporous carbon adsorbents, we have obtained HRTEM images presented in Figure 2 for CMK-1, CMK-3-100, and CMK-3-130. Figure 2A shows that the HRTEM image of the CMK-1 particle, which contains a large number of mesoporous channels interconnecting to each other in a three-dimensional ordered way. On the other hand, the HRTEM image of CMK-3-100 shows the well-ordered mesoporous channels that are arranged in a linear way whereas CMK-3-130 shows linear mesoporous channels with a slightly disordered porous network. Further, the HRTEM results also support the conclusion from XRD analysis that all the materials have ordered mesoporous structure.

Textural parameters of the nanoporous carbon materials are further obtained from low-temperature (−196 °C) nitrogen adsorption isotherms, which allow calculation of specific surface area, specific pore volume, and mesopore size distribution (see Table 1). CMK-3-130 and CMK-3-150 possess pores of diameters about 4.3 and 6.5 nm with high BET surface areas of 1250 and 1350 $m^2\ g^{-1}$ and large pore volumes of 1.3 and 1.6 $cm^3\ g^{-1}$, respectively. These values are apparently larger than those assigned to CMK-3. CMK-1 also exhibited a type IV isotherm with high uptake at low relative pressure compared to CMK-3 material, indicating the presence of micropores. The specific surface area of CMK-1 (1675 $m^2\ g^{-1}$) is higher than

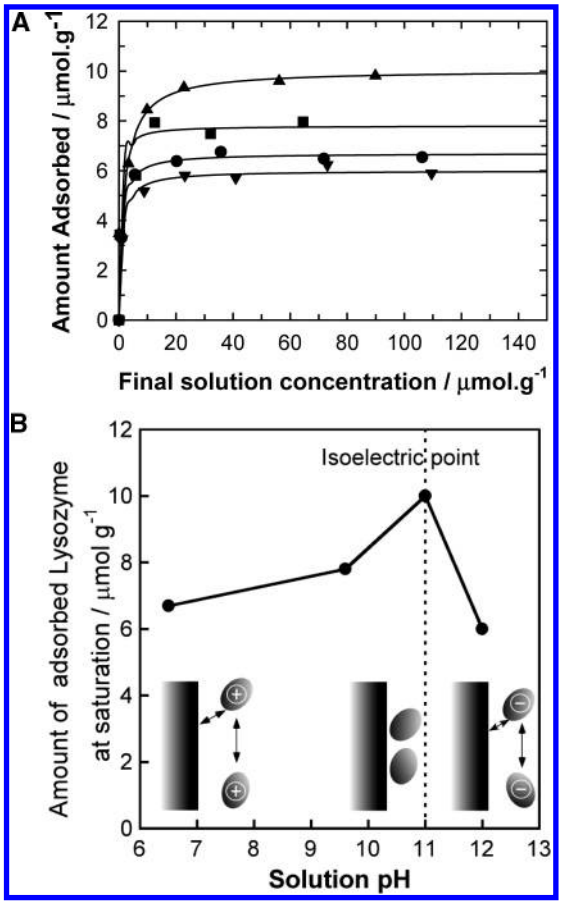

Figure 3. (A) Adsorption isotherms of Lz on CMK-3 at various pH conditions: (●) pH 6.5, (■) pH 9.6, (▲) pH 11, and (▼) pH =12.0. (B) Mechanism of adsorption of Lz over nanoporous carbon at various pH values.

the specific surface area of CMK-3-*X* materials. Among the nanoporous carbon prepared by using SBA-15-*X* as a template, CMK-3-150 exhibits very high specific pore volume and large pore diameter.

Lysozyme Adsorption: Influence of Solution pH. The adsorption isotherms of Lz on CMK-3 at different solution pH ranging from 6.5 to 12 are shown in Figure 3A. These isotherms exhibit a sharp initial rise, suggesting a high affinity between Lz and the adsorbent surface, and finally the isotherms reach a plateau, as denoted type L (Langmuir) isotherm. By employing the Langmuir model, the monolayer adsorption capacity (n_m) was calculated by using the Langmuir equation.

$$n_s = Kn_m c/(1 + Kc)$$

In this equation, *K*, *c*, and n_s represent the Langmuir constant, the Lz concentration, and the amount of the Lz adsorbed on the adsorbent, respectively. The solid lines presented in Figure 3A are the best fit Langmuir isotherm characterization of the experimental data using the above equation. Figure 3A shows that the amount of Lz adsorption increases with increasing the final solution concentration. This is due to the fact that the Lz molecule may adsorb on the solid support in various distinct orientations. At low bulk protein solution concentration, the prolate spheroid Lz molecule may be adsorbed with a side-on-type configuration perpendicular to the nanoporous carbon surface. On the other hand, when the bulk protein solution concentration is high, the protein molecules may be adsorbed with an end-on-type configuration that helps the molecules land close to each other with the long axis to reduce the increasing

electrostatic repulsion between protein molecules, resulting in a higher amount of Lz adsorption. Moreover, the high bulk concentration of Lz helps the close packing because of the decreased hydrophobic interactions between the protein and the nanoporous carbon surface upon adsorption of some Lz molecules on the carbon surface. It is also important to note that the desorption of the Lz molecule from the nanoporous carbon materials with use of 25 mM bicarbonate buffer (pH 11) was easily achieved with 70% to 90% removal of Lz from the nanoporous carbon materials.

It also can be seen from the Figure 3A that the monolayer adsorption capacity (n_m) significantly changes depending on the solution pH. The amount adsorbed increases from pH 6.5 to 10.5, but decreases when the pH is increased to 12. This trend, which has been previously observed by Vinu et al.[25] in the adsorption of Lz onto mesoporous silica molecular sieves, indicates the strong effect of solution pH on the adsorption mechanism. The maximum adsorption of Lz amounts to 9.8 μmol g^{-1} was obtained at pH 11, which is very close to the isoelectric point pI of Lz of ca. 11.[37] Near the isoelectric point, the net charge of the protein is low and the Coulombic repulsive force between the protein molecules is minimal. Consequently, a closer packing of the protein molecules is possible and the monolayer capacity increases. It is observed in Figure 3A,B that there is a large reduction in the amount of Lz adsorption on CMK-3 at pH below and above the pI. It is a well-known fact that the protein molecule is positively charged at a pH below pI and negatively charged at a pH above pI. When the solution pH is increased from 11 to 6.5, the net positive charges of the Lz molecule start to increase and so does the lateral repulsion between the Lz molecules.[38] As a consequence, the protein molecules require more space and the monolayer capacity decreases. When the solution pH is increased from 11 to 12, the surface of the Lz molecule becomes negatively charged and enhances the electrostatic repulsion between protein molecules. In our previous study on the adsorption of Lz over mesoporous silica, we reported that at pH below and above the pI, the Lz adsorption is strongly influenced by the electrostatic interaction between the negatively charged silica surface and the charged Lz molecule.[25] As the nanoporous carbon, where the surface charge is minimal, shows a similar trend in the protein adsorption amount as the negatively charged mesoporous silica, we confirm that the effect of electrostatic interaction between the adsorbent surface and Lz becomes less important with pH increase and that lateral electrostatic repulsion between the charged protein molecules is more important. Therefore, we conclude that the amount of protein adsorption with pH increase is mainly controlled by protein−protein interaction and less by protein−surface interactions.

Influence of Pore Volume and Pore Diameter. Figure 4 compares the adsorption isotherms of the Lz adsorbed on various nanoporous carbons at a solution pH of 11. As compared these curves with the structural parameters listed in Table 1, the monolayer adsorption capacity increases with increasing pore volume and pore diameter of the nanoporous adsorbents: CMK-3-150 (22.9 μmol g^{-1}) > CMK-3-130 (15.9 μmol g^{-1}) > CMK-3 (9.8 μmol g^{-1}) > CMK-1 (3.8 μmol g^{-1}). It is interesting to note that the volume occupied by the Lz molecule ($V = 17.8$ nm^3) is 15.3% of the specific pore volumes of the CMK-3-150 adsorbent determined by nitrogen adsorption, whereas only 10% and 13.1% of the specific pore volumes of the CMK-3 and CMK-3-130, respectively, was occupied by the Lz molecule. This indicates a clear increase in the amount of Lz adsorption as the specific pore volume of the nanoporous carbon material is increased.

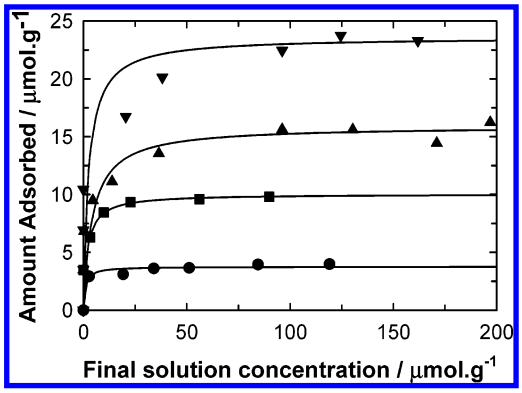

Figure 4. Adsorption isotherms of Lz on various nanoporous carbons at pH 11: (●) CMK-1; (■) CMK-3; (▲) CMK-3-130; and (▼) CMK-3-150.

It is also significant to note that only a small percentage of the specific pore volume of the nanoporous carbon is occupied by the Lz adsorption. This can be explained in two ways. First, the structure of CMK-3 is composed of ordered carbon rods, which was originally formed inside the cylindrical mesopores of the SBA-15 template. These carbon rods are rigidly interconnected by smaller carbon rods which are formed inside the micropores of main cylindrical pores of SBA-15. These smaller carbon rods may block the Lz molecule to access the interior part of the mesopores. Second, the presence of micropores in the nanoporous carbon materials restricts the diffusion of the protein molecule during adsorption. Recently, Vinu et al. have studied the microporosity analysis of different nanoporous carbons such as CMK-1, CMK-2, CMK-3, CMK-3-130, and CMK-3-150 by *n*-heptane and cyclohexane adsorption.[36] It has been found that up to 28% to 50% of micropores are present in the nanoporous carbon materials. The total amount of micropores in the CMK-3 nanoporous carbon was found to be 28%. These micropores, originating either from the incomplete polymerization of sucrose molecule inside the mesopores of the template or from the rupture of carbon−carbon bonds during pyrolysis or from the structural changes occurring during the template dissolution with hydrofluoric acid, are not useful for protein adsorption. Thus, it is not surprising that only a fraction of the specific pore volume of the nanoporous carbon was occupied by the Lz molecule. Moreover, the use of all the specific pore volume cannot be expected to correctly represent the amount of protein adsorption. It is also noted that among the carbon materials studied, CMK-1 registers a very low amount of Lz adsorption although its pore diameter is well below the molecular diameter of the Lz molecule, which demonstrates the Lz molecule is also adsorbed on the external surface of CMK-1.

Characterization of the Adsorbent after Lysozyme Adsorption. To answer the question whether the Lz molecule enters the mesopore of CMK-3, the adsorbent was also characterized by XRD and nitrogen adsorption after protein adsorption. The powder XRD patterns of CMK-3 before and after the adsorption experiment at two different initial Lz concentrations (1 and 4 g/L) at pH 11 are shown in Figure 5. All samples exhibit the XRD pattern typically observed for CMK-3, consisting of a strong (100) reflection at a low angle and two small peaks at a higher angle. The observation of these peaks even after loading the sample at a pH of 11 with ca. 9.8 μmol/g of Lz confirms retention of the hexagonal mesoporous structure. Moreover, the intensity of the low angle (100) and

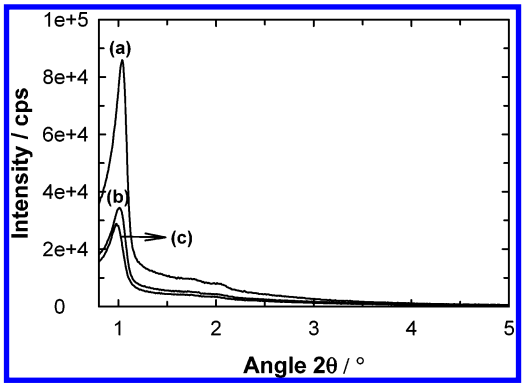

Figure 5. XRD powder patterns of CMK-3 before and after Lz adsorption at pH 11: (a) CMK-3, (b) CMK-3 (69.5 μmol/L), and (c) CMK-3 (280 μmol/L = initial concentration of Lz).

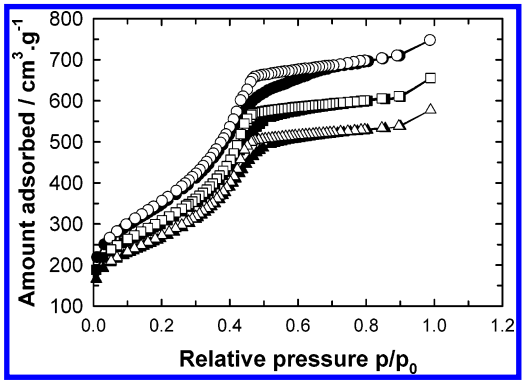

Figure 6. Nitrogen adsorption/desorption isotherms of CMK-3 (open circle, adsorption; closed circle, desorption): (●) before the Lz adsorption and at (■) 69.5 μmol/L (initial concentration of Lz) of CMK-3 and (▲) 280 μmol/L (initial concentration of Lz) of CMK-3.

high angle peaks (110 and 200) decreases as compared to the parent CMK-3 materials upon the Lz adsorption. This cannot be interpreted as a severe loss of structural order, but it is likely that larger contrast in density between the carbon walls and the open pores relative to that between the carbon walls and the Lz molecule inside the pores is responsible for the observed decrease in intensity.[39,40] Thus we assumed that the large reduction in the intensity of XRD peaks after protein adsorption is mainly due to the tight packing of Lz molecules inside the mesopores of carbon adsorbents.

N_2 adsorption isotherms of CMK-3 before and after Lz adsorption are shown in Figure 6. It is seen that the amount of nitrogen adsorbed is decreased with increasing the amount of Lz adsorption. Upon increasing the Lz loading, the specific surface area and pore volume of CMK-3 are decreased from 1300 to 930 m^2/g and 1.05 to 0.85 cm^3/g, respectively. The actual volume of the Lz adsorbed is only 0.1 cm^3/g (assuming the net volume of one Lz molecule = 17.8 nm^3), which is 10% of the total free volume of CMK-3 materials, while the nitrogen adsorption measurement shows almost 19% reduction in the specific pore volume of CMK-3. Moreover, the difference between the pore volume occupied by the adsorbed Lz molecule calculated from the theoretical and the nitrogen adsorbed data is only 9% in CMK-3, while more than 45% difference was observed in mesoporous silica.[25,26] The large difference in the later case is mainly due to the partial structural collapse of mesoporous silica after the adsorption of protein at higher pH where the possibility of the hydrolysis of siloxane bridges in the mesoporous silica is very high. The reduction in the specific mesopore volume after Lz adsorption clearly indicates that the Lz molecules are adsorbed inside the mesopores of CMK-3 adsorbent without affecting the structural integrity of the parent materials. All the above data clearly demonstrate that nanoporous carbon is the best adsorbent choice for the protein adsorption and is more stable as compared to the mesoporous silica after the protein adsorption.

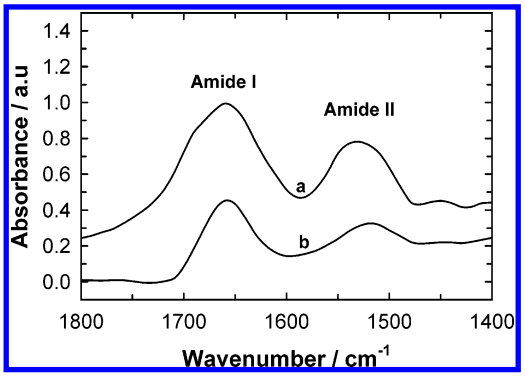

Figure 7. FT-IR spectra of the pure Lz (a) and Lz loaded on CMK-3 (b).

To confirm the structural stability of the Lz after adsorption on the nanoporous carbon, Transmission FT-IR spectra were recorded for the Lz loaded nanoporous adsorbents CMK-3 in comparison to pure lysozyme. Figure 7a shows the typical Transmission FT-IR spectrum for lysozyme recorded at room temperature. The amide bands I and II are generally employed to study the protein structure. The amide band I (near 1657 cm^{-1}) is due to the C═O stretching mode, whereas the amide II band (near 1527 cm^{-1}) is due to the stretching mode of N−H vibrations. Typically, the disappearance of the amide II N−H stretching mode is used to follow the unfolding of the protein. Figure 7b also shows the Transmission FT-IR spectrum of Lz adsorbed on nanoporous carbon after subtraction of the spectrum of unloaded CMK-3. The spectra also show two major bands centered at 1657 and 1527 cm^{-1}. The intensity ratio between these two bands did not virtually alter upon adsorption of the Lz onto the nanoporous carbon. It can be assumed that the Lz molecules are tightly packed inside the nanopores of CMK-3 and do not have room for changing their structural confirmation inside the nanoporous matrix. These results indicate the absence of serious denaturation accompanying changes in secondary structures (α-helix and β-sheet) through the adsorption process.[41,42]

Conclusions

Adsorption of Lz over nanoporous carbons with various pore diameters has been studied under various pH conditions. It has been found that the amount of Lz adsorbed depends on the solution pH as well as the specific pore volume of the adsorbent. The maximum amount of Lz has been achieved for CMK-3 near the isoelectric point of the protein where the zero net charge of the Lz molecule causes no electrostatic repulsion. It has also been found that the amount adsorbed is mainly a function of the pore diameter and the specific pore volume. XRD and nitrogen adsorption data after the protein adsorption revealed that the Lz molecule is adsorbed inside the channels of nanoporous adsorbents. The above data also confirmed the unaltered structural order of the CMK-3 nanoporous carbon even after the protein adsorption at higher pH. FT-IR spectra of the adsorbed Lz confirmed that the adsorption of the Lz did not result in denaturation of the protein.

Acknowledgment. This work was partially financed by Special Coordination Funds for Promoting Science and Tech-

nology from the Ministry of Education, Culture, Sports, Science and Technology of the Japanese Government.

References and Notes

(1) Lvov, Y.; Möhwald, H. *Protein Architecture;* Marcel Dekker: New York, 1999.

(2) Rusling, J. F. *Biomolecular Films: Design, Function and Applications*; Marcel Dekker: New York, 2003.

(3) Malmsten, M. *Biopolymers at Interfaces, Revised and Expanded*; Marcel Dekker: New York, 2003.

(4) Lvov, Y.; Ariga, K.; Ichinose, I.; Kunitake, T. *J. Am. Chem. Soc.* **1995**, *117*, 6117.

(5) Onda, M.; Lvov, Y.; Ariga, K.; Kunitake, T. *J. Ferment. Bioeng.* **1996**, *82*, 502.

(6) Onda, M.; Lvov, Y.; Ariga, K.; Kunitake, T. *Biotechnol. Bioeng.* **1996**, *51*, 163.

(7) Okahata, Y.; Tsuruta, T.; Ijiro, K.; Ariga, K. *Langmuir* **1988**, *4*, 1373.

(8) Okahata, Y.; Tsuruta, T.; Ijiro, K.; Ariga, K. *Thin Solid Films* **1989**, *180*, 65.

(9) Yanagisawa, T.; Shimizu, T.; Kuroda, K.; Kato, C. *Bull. Chem. Soc. Jpn.* **1990**, *63*, 988.

(10) Kresge, C. T.; Leonowicz, M. E.; Roth, W. J.; Vartuli, J. C.; Beck, J. S. *Nature* **1992**, *359*, 710.

(11) Sayari, A.; Hamoudi, S. *Chem. Mater.* **2001**, *13*, 3151.

(12) Davis, M. E. *Nature* **2002**, *417*, 813.

(13) Okabe, A.; Fukushima, T.; Ariga, K.; Aida, T. *Angew. Chem., Int. Ed.* **2002**, *41*, 3414.

(14) Hartmann, M.; Vinu, A. *Langmuir* **2002**, *18*, 8010.

(15) Hartmann, M.; Vinu, A.; Elangovan, S. P.; Murugesan, V.; Böhlmann, W. *Chem. Commun.* **2002**, 1238.

(16) Vinu, A.; Murugesan, V.; Hartmann, M. *Chem. Mater.* **2003,** *15*, 1385.

(17) Joseph, T.; Deshpande, S. S.; Halligudi, S. B.; Vinu, A.; Ernst, S.; Hartmann, H. *J. Mol. Catal. A* **2003**, *206*, 13.

(18) Ariga, K. *Chem. Rec.* **2004**, *3*, 297.

(19) Zhang, Q.; Ariga, K.; Okabe, A.; Aida, T. *J. Am. Chem. Soc.* **2004**, *126*, 988.

(20) Vinu, A.; Hartmann, M. *Chem. Lett.* **2004**, *33*, 588.

(21) Vinu, A.; Usha Nandhini, K.; Murugesan, V.; Böhlmann, W.; Umamaheswari, V.; Pöppl, A.; Hartmann, M. *Appl. Catal. A*: *General* **2004**, *265*, 1.

(22) Karthik, M.; Tripathi, A. K.; Gupta, N. M.; Vinu, A.; Hartmann, M.; Palanichamy, M.; Murugesan, V. *Appl. Catal. A*: *General* **2004**, *268*, 139.

(23) Karthik, M.; Tripathi, A. K.; Gupta, N. M.; Vinu, A.; Palanichamy, M.; Murugesan, V. *Microporous Mesoporous Mater.* **2004**, *70*, 15.

(24) Vinu, A.; Murugesan, V.; Böhlmann, W.; Hartmann, M. *J. Phys. Chem. B* **2004**, *108*, 11496.

(25) Vinu, A.; Murugesan, V.; Hartmann, M. *J. Phys. Chem. B* **2004**, *108*, 7323.

(26) Vinu, A.; Murugesan, V.; Tangermann, O.; Hartmann, M. *Chem. Mater.* **2004**, *16*, 3056.

(27) Lu, K.; Chung, D. D. L. *Carbon* **1997**, *35*, 427.

(28) Ryoo, R.; Joo, S. H.; Jun, S.; *J. Phys. Chem. B* **1999**, *103*, 7743.

(29) Lee, J.; Yoon, S.; Hyeon, T.; Oh, S. M.; Kim, K. B. *Chem. Commun.* **1999**, 2177.

(30) Jun, S.; Joo, S. H.; Ryoo, R.; Kruk, M.; Jaroniec, M.; Liu, Z.; Ohsuna, T.; Terasaki, O. *J. Am. Chem. Soc.* **2000**, *122*, 10712.

(31) Ryoo, R.; Joo, S. H.; Kruk, M.; Jaroniec, M. *Adv. Mater.* **2001**, *13*, 677.

(32) Joo, S. H.; Choi, S. J.; Oh, I.; Kwak, J.; Liu, Z.; Terasaki, O.; Ryoo, R. *Nature* **2001**, *412*, 169.

(33) Lee, J.; Han, S.; Hyeon, T. *J. Mater. Chem.* **2004**, *14*, 478.

(34) Vinu, A.; Streb, C.; Murugesan, V.; Hartmann, M. *J. Phys. Chem. B* **2003**, *107*, 8297.

(35) Han, S.; Kim, S.; Lim, H.; Choi, W.; Park, H.; Yoon, J.; Hyeon, T. *Microporous Mesoporous Mater.* **2003**, *58*, 131.

(36) Vinu, A.; Hartmann, M. *Catal. Today.* In press.

(37) Wilson, K. P.; Malcolm, B. A.; Matthews, B. W. *J. Biol. Chem.* **1992**, *267*, 10842.

(38) Haynes, C. A.; Norde, W. *Colloids Surf. B* **1994**, *2*, 517.

(39) Marler, B.; Oberhagemann, U.; Vortmann, S.; Gies, H. *Microporous Mesoporous Mater.* **1996**, *6*, 375.

(40) Hammond, W.; Prouzet, E.; Mahanti, S. D.; Pinnavaia, T. J. *Microporous Mesoporous Mater.* **1999**, *27*, 19.

(41) Caruso, F.; Furlong, D. N.; Ariga, K.; Ichinose, I.; Kunitake, T. *Langmuir* **1998**, *14*, 4559.

(42) Adams, S.; Higgins, A. M.; Jones, R. A. L. *Langmuir* **2002**, *18*, 4854.